An *in vitro* method for inducing titan cells reveals novel features of yeast-to-titan switching in the human fungal pathogen *Cryptococcus gattii*

Lamin Saidykhan[1,3], Joao Correia[1], Andrey Romanyuk[1,2], Guillaume E. Desanti[1], Leanne Taylor-Smith[1], Maria Makarova[1], Elizabeth R. Ballou[1*], Robin C. May[1*]

[1]Institute of Microbiology & Infection and School of Biosciences, University of Birmingham, Edgbaston, Birmingham, United Kingdom.

[2]School of Chemistry, University of Birmingham, Edgbaston, B15 2TT Birmingham, UK.

[3]Division of Physical and Natural Science, University of The Gambia, Brikama Campus, West Coast Region, The Gambia.

***Correspondence should be addressed to e.ballou@exeter.ac.uk or r.c.may@bham.ac.uk**

Abstract

Cryptococcosis is a potentially lethal fungal infection of humans caused by organisms within the *Cryptococcus neoformans/gattii* species complex. Whilst *C. neoformans* is a relatively common pathogen of immunocompromised individuals, *C. gattii* is capable of acting as a primary pathogen of immunocompetent individuals. Within the host, both species undergo morphogenesis to form titan cells: exceptionally large cells that are critical for disease establishment. To date, the induction, defining attributes, and underlying mechanism of titanisation have been mainly characterized in *C. neoformans*. Here, we report the serendipitous discovery of a simple and robust protocol for *in vitro* induction of titan cells in *C. gattii*. Using this *in vitro* approach, we reveal a remarkably high capacity for titanisation within *C. gattii,* especially in strains associated with the Pacific Northwest Outbreak, and characterise strain-specific differences within the clade. In particular, this approach demonstrates for the first time that cell size changes, DNA amplification, and budding are not always synchronous during titanisation. Interestingly, however, exhibition of these cell cycle phenotypes was correlated with genes associated with cell cycle progression including *CDC11, CLN1, BUB2,* and *MCM6.* Finally, our findings reveal exogenous p-Aminobenzoic acid to be a key inducer of titanisation in this organism. Consequently, this approach offers significant opportunities for future exploration of the underlying mechanism of titanisation in this genus.

Introduction

C. neoformans and *C. gattii* are two pathogenic species of *Cryptococcus* that cause invasive cryptococcosis in immunocompromised patients as well as immunocompetent individuals [1-3]. Upon inhalation into the lungs, *Cryptococcus* is exposed to a repertoire of hostile host factors (e.g., elevated temperature, nutrient deprivation, higher physiological CO_2 and hypoxia), [4, 5] which trigger adaptive phenotypes such as the formation of titan cells. Titan cell formation is a dramatic morphological change as cryptococcal haploid yeast cells (5-7µm) transform into enormous polyploid titan cells (50-100µm in diameter) [6, 7]. This atypical morphotype is characterized by many attributes such as enlarged cell size, thicker cell wall, and altered capsule composition, which confer resistance to host immune defence and enhance survival in the host [8-10].

C. neoformans titan cells have been clinically observed [11, 12], studied *in vivo* [6, 7] and recently induced *in vitro* [13-15]. The discovery of *in vitro* induction protocols is considered a major breakthrough, as efforts employed towards understanding the biology and mechanism underlying titanisation were impeded by the ethical and technical challenges associated with using animal models. Although titanisation is also thought to be a major virulence factor of *C. gattii* [16-18], the defining attributes and underlying mechanism of titanisation have thus far been mainly characterized in *C. neoformans* [19-23].

Here we describe a facile *in vitro* induction approach that reveals a novel strategy for titanisation in *C. gattii*. Specifically, this method reveals that the *C. gattii*/VGIIa strain R265 deviates from the usual synchronous occurrence of cell enlargement and polyploidization that occurs in *C. neoformans.* Instead, R265 delays DNA endoreduplication, growing to around 30µm as a haploid cell over the first 3 days of induction before endoreduplicating its DNA to become a uninucleate polyploid cell. Secondly, unlike *C. neoformans*, R265 titan cells produce

daughter cells before reaching their critical cell size, after which they permanently cease budding unless they are exposed to conditions compatible with normal yeast growth. Although occurrence of these cell cycle phenotypes is asynchronous, these behaviors during titanisation are correlated with the expression levels of genes associated with cell cycle progression such as *CLN1, CDC11, MCM6* and *BUB2.* By studying offspring from crosses between R265 and other *C. gattii* strains, we show that the propensity to titanise is most likely a highly polygenic trait and identify a number of hybrid strains in which *in vitro* titanisation levels approach 100%, opening the door to future molecular studies of this biological phenomenon.

Finally, we discovered that the widespread metabolite and UV-scavenger p-Aminobenzoic acid (pABA) is required for maximal titanisation *in vitro*, providing a molecular inroad to future investigations of the titanisation pathway.

Results

Titan cells are induced by growth in RPMI medium

While characterizing co-culture of *C. gattii* with an alveolar macrophage cell line (MH-S) at a low multiplicity of infection (MOI [5:1]), we made the serendipitous discovery that exposure of low density R265 cultures to sterile RPMI growth media at 37°C in an atmosphere of 5% CO_2 induced dramatic cell size increase within 24 hrs (Fig. 1A and B). Extending the incubation period to seven days enabled these giant cells to achieve cell bodies of up to 30µm in diameter, resulting in a population with a median size two-fold larger than yeast cells grown in YPD overnight [median size: 13.7µm (5.1-29.8) vs 5.8µm (4.0 -7.6); ($p<0.0001$)] (Fig. 1C and 1E [α=cell body diameter]).

The cryptococcal yeast-titan transition occurs concomitantly with increasing capsule thickness [16]. Therefore, we characterized the capsule size (Fig. 1D and 1E [ß=capsule size]) of our *in*

vitro-generated R265 giant cells. Relative to the YPD-grown capsule thickness, R265 giant cells demonstrated significantly thicker capsule [median capsule thickness: 10.28µm (0.34-22.9) vs 1.00µm (0.2-3.1), p<0.0001]. Although the cell body size progressively increased with induction time from 24 hr to 7 days (Fig. 1C), the capsule size of the giant cells reached a plateau at 24 hours and remained at a median size of 10.33µm (1.0-22.9) for the remaining six days of the assay (Fig. 1D). This suggests that the giant cells achieve their maximum capsule size much earlier than their maximum cell body size. In addition to displaying a titan-like capsule and cell body, *C. gattii* (R265) giant cells bear a single large vacuole occupying almost the entire protoplasmic space (Fig. 1E), a characteristic previously described with *in vivo* and *in vitro*-derived *C. neoformans* titan cells [7, 13].

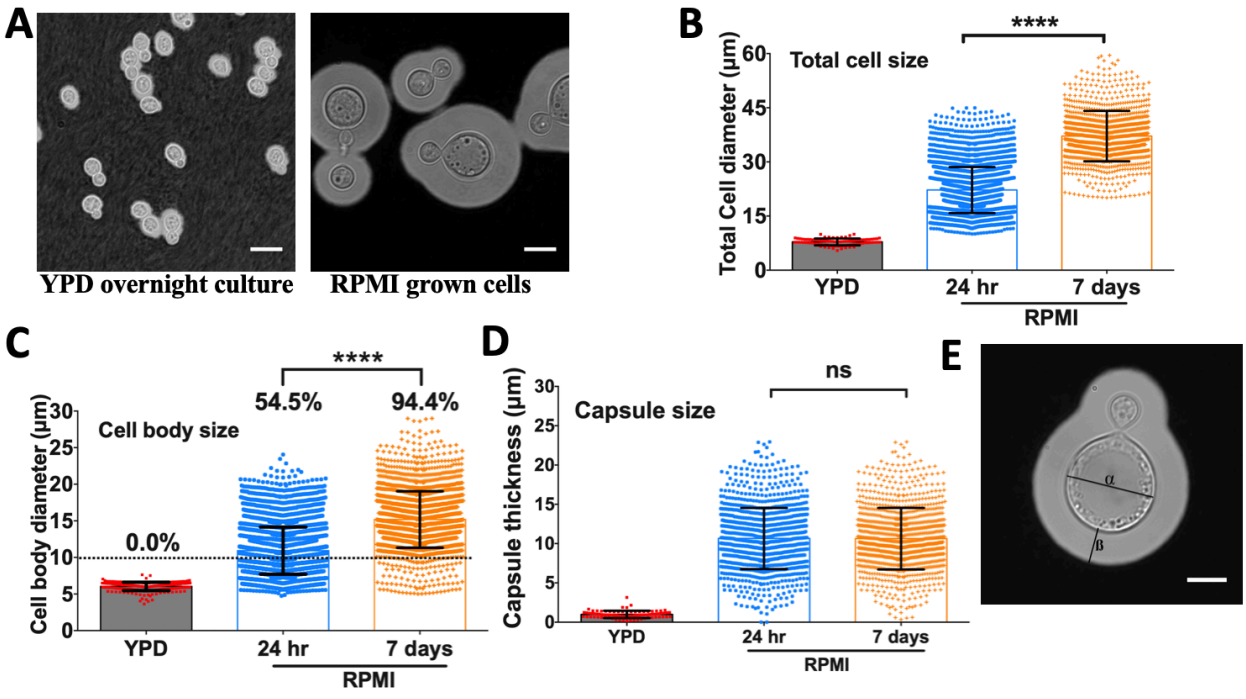

Figure 1: *C. gattii* (R265) exhibits cell body and capsule enlargement in response to growth in RPMI. A) Micrographs of R265 cells grown overnight in YPD at 25°C in atmospheric conditions (left panel) and grown in RPMI at low density for 24 hrs at 37 °C in an atmosphere of 5% CO_2 (right panel). Scale bar=15µm. B) Total cell diameter (capsule included), C) cell body diameter (percentages represent percentage of cells more than 10µm in

diameter) and D) capsule thickness of R265 cells all significantly increase after growth in RPMI at 37°C in 5% CO_2. The graphs represent at least 3 biological experimental repeats, and a one-way ANOVA was used to determine significance where **** = $p<0.0001$. E) Cellular morphology of R265 giant cells: cell body diameter (α) and capsule thickness (ß).

Titan cells exhibit altered cell wall composition [13, 15, 24]. Consequently, we characterized the cell wall of R265 *in vitro*-derived giant cells by staining for chitin with calcofluor white (CFW, Fig. 2A) [15]. In line with previous studies, we observed a significant increase ($P<0.05$) in the chitin content of giant induced cells via flow cytometry (Fig 2B and 2C) that was also evident via fluorescence microscopy (Fig. 2A).

In addition to changes in cellular morphology, the yeast-titan transition in *C. neoformans* involves a switch from a haploid to highly polyploid state [6, 7, 13, 15]. Thus, we evaluated the ploidy of RPMI *in vitro*-generated *C. gattii* giant cells. Whilst YPD grown yeast cells typically displayed a mix of cells with 1C or 2C DNA content (depending on which phase of the cell cycle they are in), RPMI-induced cells displayed DNA content ranging up to 16C after 7 days of induction (Fig. 2D). By DAPI staining the nucleus and visualizing by microscopy, we confirmed the giant cells were uninucleate (Fig. 2E). Thus, R265 titan-induced cells exhibit all the key features of bona fide titan cells: cell enlargement, a large vacuole, altered cell wall composition and high ploidy. Interestingly, however, we noted that in the case of R265, cell enlargement and increased DNA content do not necessarily occur at the same time. Indeed, R265 cells achieve significant cell body enlargement within 24hrs, but DNA content does not exceed 2C until much later (Fig. 2D). Taken together, the structural attributes exhibited by the *in vitro* RPMI-induced titan cells are typical of true titan cells.

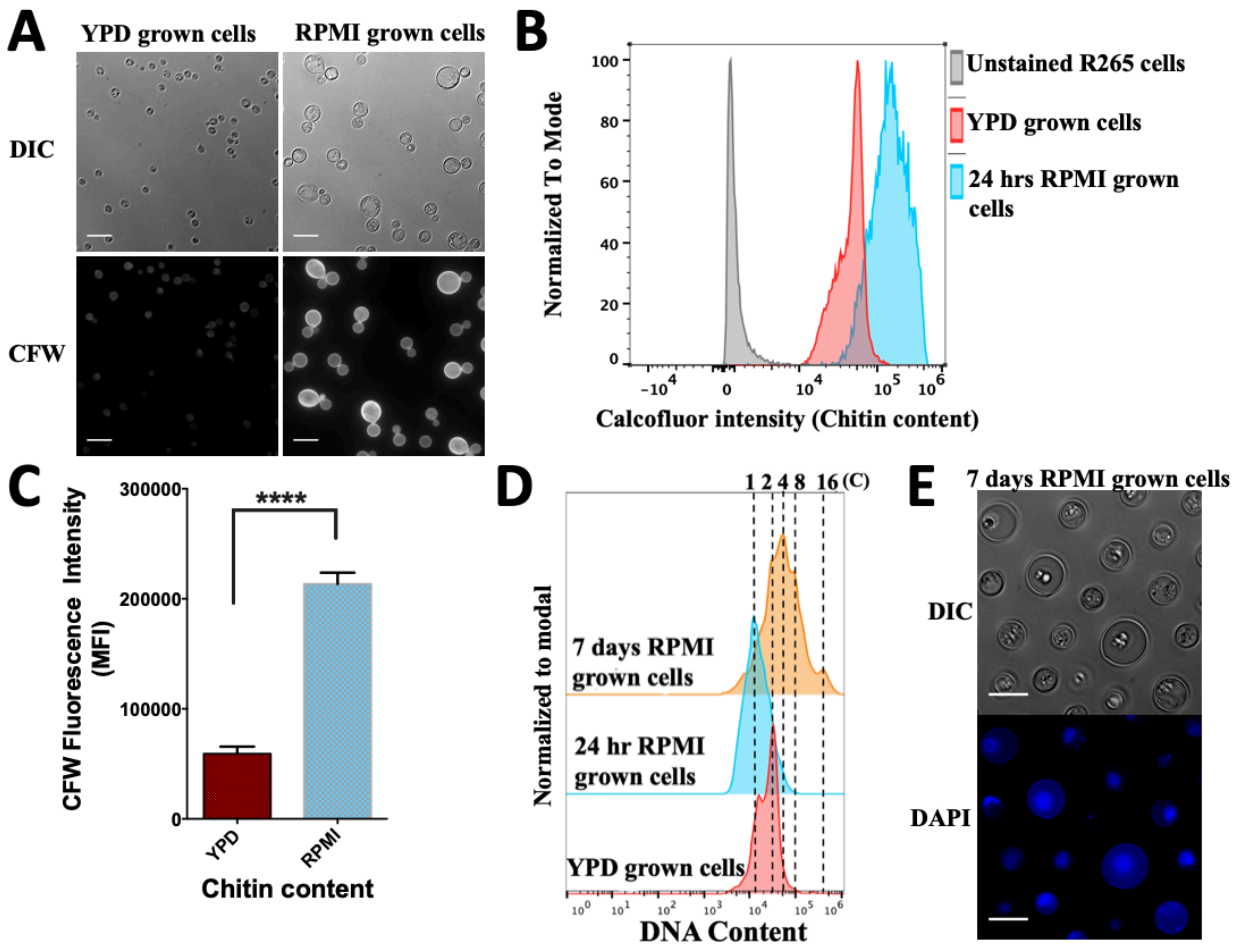

Figure 2: The cell wall chitin content and ploidy of enlarged cells are typical of titan cells. *In vitro* RPMI-generated giant cells displayed a significantly higher chitin level relative to YPD grown R265 cells, as indicated by the calcofluor white (CFW) fluorescence intensity shown using microscopy imaging in (A), via flow cytometry in (B) and graphically in (C, Median Fluorescence Intensity, MFI) ($p<0.05$). Scale bar=15µm. Statistical significance was confirmed by Two-tailed *t*-test. D) Ploidy measurement of RPMI-generated giants cells based on flow cytometry analysis of DAPI staining. YPD grown cells (red) gated as 1C, 2C (haploid) were used as a control to determine ploidy (DNA content) of enlarged cells after 24 hr (blue) and 7days (orange) of induction. E) Micrographs showing the uninucleate nature of R265 titan cells upon staining with DAPI to visualize the nucleus. Scale bar=15µm.

In R265, cell enlargement is asynchronous with ploidy

To characterise the kinetics of cell size and ploidy changes more fully, we carried out a detailed time course analysis of R265 cells over a period of three weeks. By day 3 of induction, R265 cells showed significantly enlarged body diameter as compared with non-induced (YPD grown) cells [median size: 13.7µm (5.1-29.8) vs 6.5µm (4.9-8.89); ($p<0.0001$)] with 81.5% (5241/6431) of cells larger than 10µm (Fig. 3A). Despite this size increase, for the first three days all cells were 1C or 2C (reflecting a haploid cell cycle) (Fig 3B). The population reached the maximum cell size on day 5, and from day 5 to day 7, there was no change in the size of induced cells [median size being 14.9µm at day 5 and 14.7µm at day 7]. However, the ploidy of these cells increased, with tetraploid (4C) cells apparent at day 5 and cells exhibiting DNA content of up to 16C by day 7. In parallel, although the maximum size of induced cells no longer increased at this late stage of incubation, the proportion of the population with a large cell phenotype rose from 92.8% to 99.3% ($p<0.0001$) (Fig 3A). Thus, it appears that: a) size increase and ploidy increase are separable phenotypes during titanisation of R265, b) true titan cells (large and polyploid) appear only after around 5 days of induction and c) their maximum cell size is achieved rapidly during titanisation, but the proportion of cells adopting this fate rises steadily over a long time period.

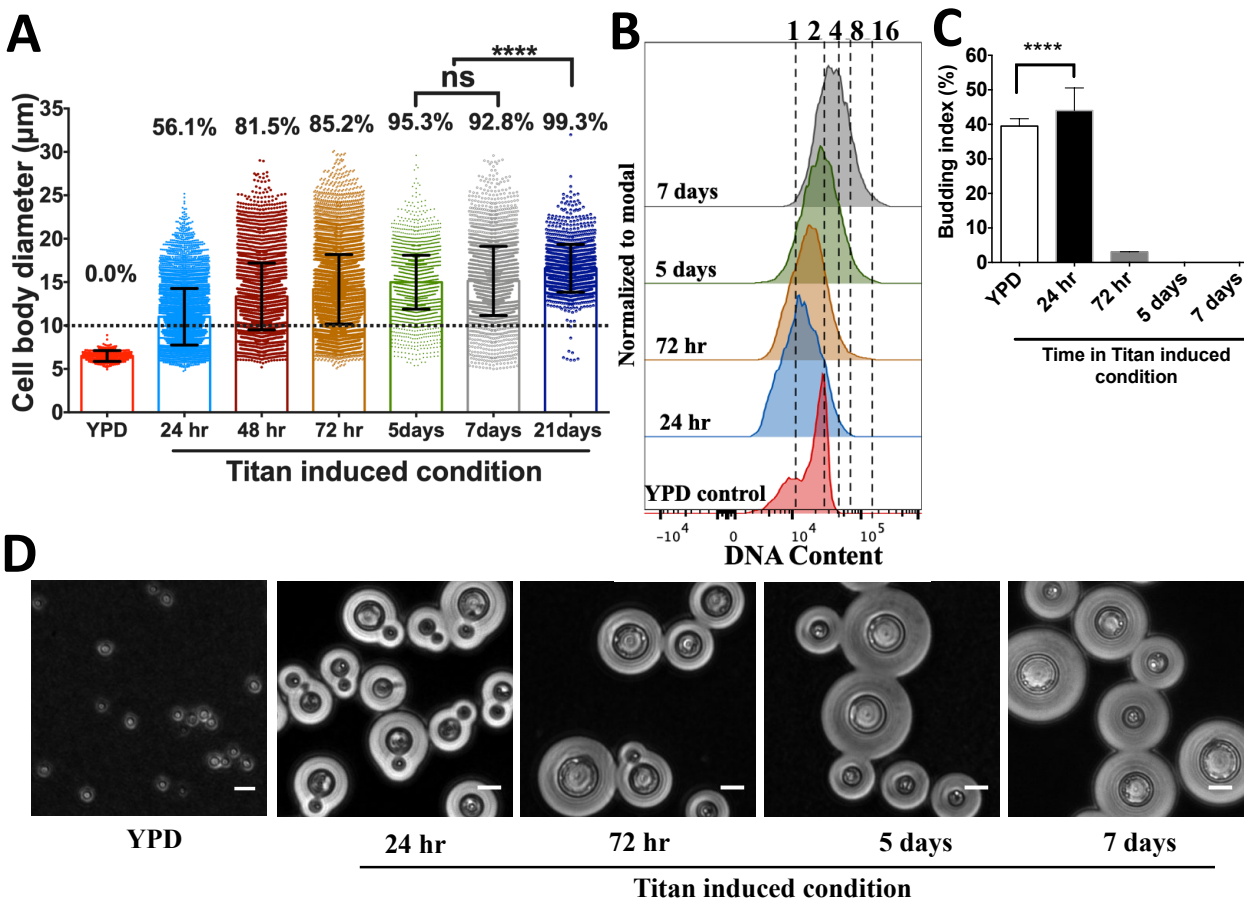

167

168

169 **Figure 3 Cell enlargement, polyploidization and budding occur at different periods**
170 **during titan induction in R265.** A) Cell body diameter of R265 titan cells over prolonged
171 induction (24 hr to 21 days) as compared to YPD grown cells. Enlarged cells were recovered
172 from induction conditions at different time points, fixed and measured. The graphs are
173 representation of 3 biological repeats and statistical significance was determined by one-way
174 ANOVA, where ****=$p<0.05$. B) Samples from all the induction time points were fixed, DAPI
175 stained and analysed for ploidy by flow cytometry with reference to YPD grown cells, which
176 were used to gate for 1C and 2C DNA content. C) Budding index of cells recovered from YPD
177 and titan inducing condition. Budding index was expressed as percentage of budded cells per
178 total number of cells. At least 3000 cells were analysed for each sample (the graph represents
179 three biological repeats and significance was confirmed by one-way ANOVA where,

****=p<0.05. D) Microscopy images showing the budding nature of cells obtained from YPD or at various timepoints after titan induction. Scale bar: 15µm.

The polyploid titan cells are unbudded

Within our *in vitro* model, after 3 days of induction, the R265 titan cells completely stop budding despite being polyploid [Fig. 3]. This suggests that budding and DNA increase are decoupled, consistent with endoreduplication. During the first 3 days, the budding index (the number of mother cells producing buds) fell from 44.4% (2552/5749 cells) at 24 hr to 2.8% (26/933) by day 3 and 0% (0/2971) by the fifth day of induction (Fig. 3C). Hence, we termed the period before 3 days of induction as the budded phase and the later period as the unbudded phase. During the budded phase, cells predominantly exhibited a 1C DNA content (Fig. 3B and Fig. 3D). However, during the unbudded phase (3 to 7 days) cells rapidly became polyploid, with DNA content rising from 2C to 4C to 16C (Fig. 3B and Fig. 3D). The 1C DNA content during the budded phase, coupled with cell enlargement, suggests that the cells spend longer in the G1 phase of their cell cycle during titan induction.

The unbudded titan cells emerge slowly from growth arrest and produce yeast-like daughter cells.

The unbudded state of *C. gattii* (R265) titan cells prompted us to investigate whether this cell cycle arrest occurs as a consequence of nutrient deprivation. By filtering 7 day old titan-induced cultures, we obtained the largest (>20µm) titan cells and re-cultured them on a rotary wheel at 20 rpm for i) 2 hr or ii) overnight at 25°C in YPD broth. These cells remained unbudded during the first 2 hrs (the generation period of *Cryptococcus* yeast) (Fig. 4A) but after overnight incubation produced daughter cells (Fig. 4B) resembling yeast cells in size and morphology (round-shaped with small capsule size) (Fig. 4C and Fig. 4D). Time-lapse observation revealed that titan cells starts budding after 2 hours (Video S1).

206

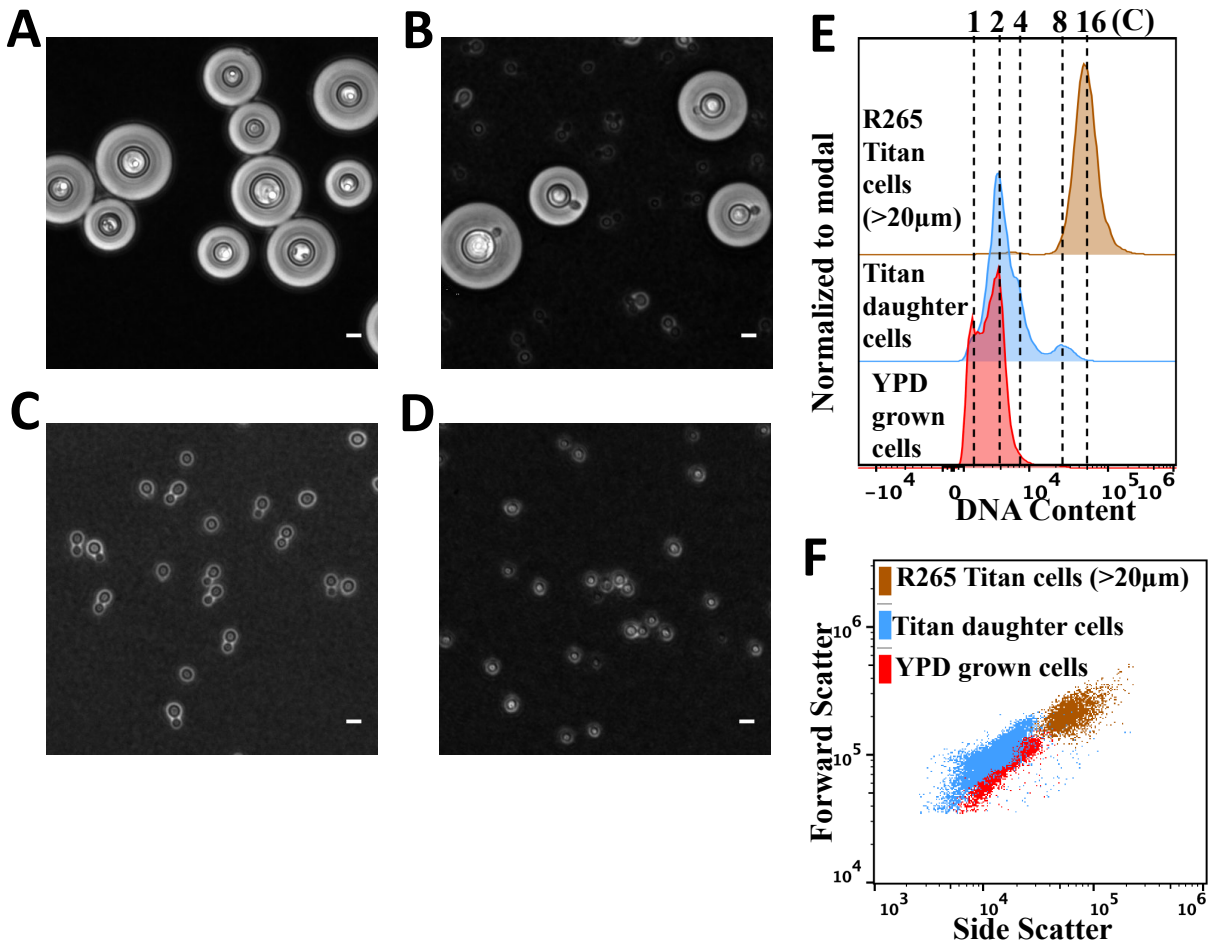

207

208 **Figure 4 Characterization of daughter cells of R265 titan cells.** 7 day old R265 titan cells
209 were purified using a 20µm cell strainer (A) and then B) re-cultured overnight in YPD to induce
210 budding. C) After 24hrs, daughter cells of R265 titan cells were isolated by filtration of the
211 titan culture (through a >15µm cell strainer) and microscopically compared with D) YPD
212 grown yeast R265 cells (control). Scale bar =10µm. E) DNA content of titan-derived daughter
213 cells (Blue) cells as compared to YPD grown (red) and >20µm R265 titan cells (brown). F)
214 Size distribution of daughter cells (blue), YPD grown (red) and >20µm R265 titan cells
215 (brown).

216

217 **Titan cells produce polyploid, yeast-sized, daughter cells**

218 To investigate if the cellular similarities observed between titan-derived daughter cells and
219 yeast cells extend to their ploidy, we characterized the DNA content of daughter cells relative

to their highly polyploid titan mother cells (>20μm) and haploid yeast cells. Despite having the cellular properties of yeast cells (Fig. 4C, 4D and 4F), titan-derived daughter cells exhibited a higher DNA content than normal yeast, with most cells displaying either diploid (2C) or polyploid (>4C) DNA content (Fig. 4E). Taken together, the delayed DNA replication of R265 titan cells (Fig. 3B) coupled with the production of polyploid daughter cells (up to 8C) (Fig. 4E) is indicative of high ploidy elasticity in *C. gattii* titan cells.

By re-culturing titan-derived daughter cells in titan inducing condition, we assessed the ability of these 'second generation' cells to return to a titan state. Unlike the 'original' titan cells, these titan-derived daughters increased their DNA content within 24 hours, achieving genome sizes of 16C and 32C at 24hr and 7 days respectively (Fig. S1C and S1D). As with the original mother titan cells, titan-induced daughter cells underwent budding during the early induction period but formed unbudded titan cells by day 7 of induction (Fig. S1A and S1B).

The titan cell cycle phenotypes are correlated with the expression of genes involved in cell cycle progression

The manner in which R265 progressively exhibits cell-cycle-associated phenotypes (cell enlargement, budding, DNA replication and finally growth arrest) to form unbudded polyploid titan cells led us to question the underlying cell cycle regulatory mechanism. We extracted RNA from R265 titan induced cells between 24 hr and 7 days of our *in* vitro protocol and then investigated the expression of a panel of cell cycle markers via quantitative RT-PCR (Table S1).

In line with the phenotypic changes that we observe during titan cell formation, the cell cycle markers we examined showed a clear shift from budding and mitosis to DNA replication and eventually cell-cycle arrest (Fig. 5). Thus, the *CDC11* gene, encoding a septin protein involved in bud formation, was highly expressed in YPD grown cells and for the first 24hrs of induction,

246 but downregulated in the "unbudded phase" timepoints (Fig. 5A). The expression of the G1
247 cyclin *CLN1* similarly was reduced at day 3 compared to 24 hrs, while expression was
248 somewhat restored by day 5 (Fig. 5B). In contrast, *MCM6* and *BUB2,* associated with DNA
249 replication and G2 arrest respectively, both peaked at 7 days where the titan cells exhibit
250 maximum polyploidy and remain unbudded (Fig. 5C and Fig. 5D).
251

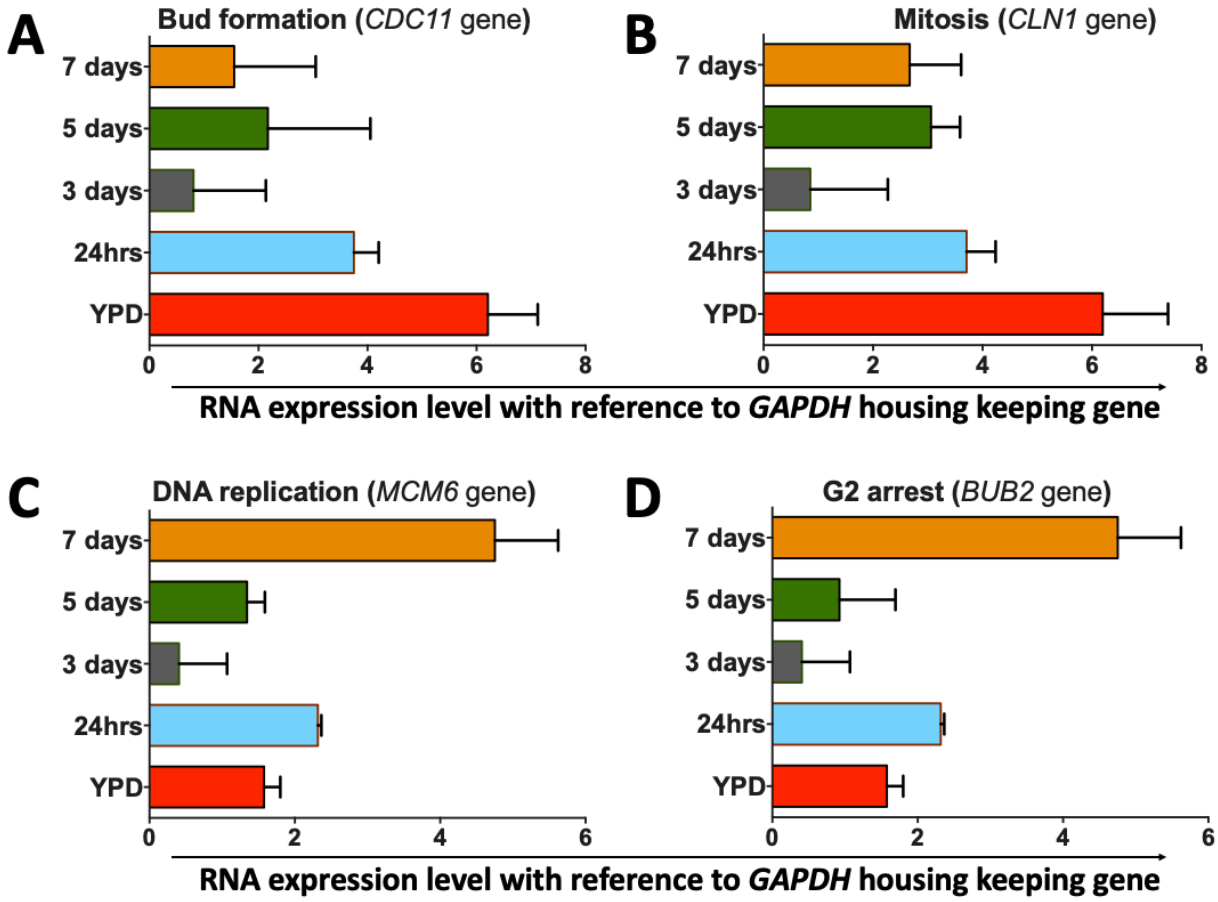

252

253 Figure 5 **Transcription profile of R265 cell-cycle-regulating genes during titanisation.**
254 Quantitative expression analysis of four different cell cycle associated genes in R265 grown in
255 either YPD (control) or titanising conditions for the indicated time points. Expression is shown
256 relative to the housekeeping gene GAPDH. Genes quantified were A) *CDC11* (*CNBG_5339)*,
257 involved in bud formation; B) *CLN1 (CNBG_4803)*, associated with balancing cell division
258 and DNA replication [25]; C) *MCM6 (CNBG_5506*), involved in DNA replication; and D)

BUB2 (CNBG_4446), involved in G2 arrest. The graphs represent 3 biological repeats (3 technical replicates each), with error bars depicting the standard deviaion of *delta-delta* C_T values.

Titan cell formation is inversely correlated to cell density

Previous work in *C. neoformans* has shown that titan cells are preferentially produced at low cell density [7, 14, 15, 26]. We tested whether the same was true of R265 by growing yeast cells in RPMI at five decreasing inoculum concentrations (10^6, $5x10^5$, $5x10^4$, $5x10^3$ and 10^3 cells/mL) and incubating for 24hr at 37°C in 5% CO_2. The formation of titan cells was maximal [14.0% titan cells (408/2999) >15µm] at an initial inoculum of $5x10^3$ cells/mL, producing cells with a median cell body size of 10.5µm (4.2-26.28) (Fig. 6A)**.** The percentage of titan cells decreased with increasing cell densities, indicating that in *C. gattii*, as in *C. neoformans*, titan induction occurs primarily in low density cultures.

High density growth in RPMI produces large, haploid, non-titan cells

The impact of culture density led us to ask what happens to R265 in non-titanising (high density) conditions. To answer this, we inoculated R265 cells in RPMI at 10^6 cells/mL and measured cell body size, capsule size, and ploidy over 7 days. At high density, there was a statistically significant increase in cell body size from 24 hr to 7days (median size: 9.0µm vs 10.5µm, $p<0.0001$) (Fig 6B), but they did not become the very large titan cells that appear in low density cultures (Fig. 1C). At both time points in these high-density conditions, cell enlargement reached a maximum threshold of 15µm with 0.1% (4/4302) and 1.3% (46/3489) of cells scoring >15µm at 24 hr and 7 days respectively (Fig. 6B). The 7-day cultures were fully growth-arrested, as evidenced by their very low budding index of 2.1% (67/3122) (Fig. 6C and Fig 4E). Interestingly, however, these 7-day, non-titan cells displayed a dramatic capsule size increase as compared to YPD grown cells (Fig 6E), perhaps due to the effect of

285 RPMI media and CO_2, which have been employed for capsule induction in *Cryptococcus* [16,
286 27-29]. Interestingly, unlike cells grown in low-density titan-inducing conditions, cells grown
287 at high density remained haploid over the entire 7 day period (Fig 4D). We conclude that high-
288 density long-term culture in RPMI induces a degree of cell enlargement in R265, but these
289 large cells are distinct from the true titans that appear in low density culture.

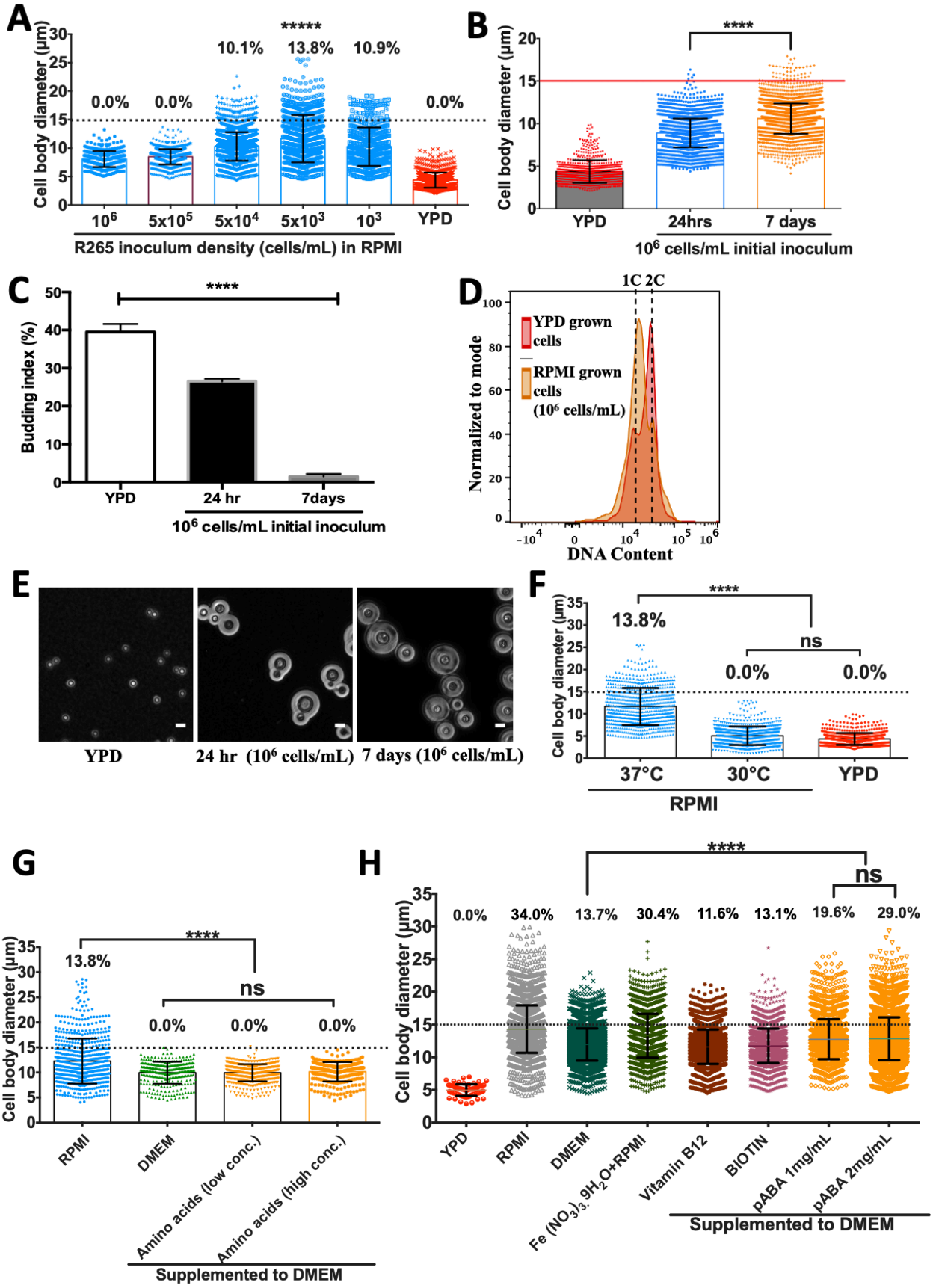

Figure 6 Effect of cell density, environmental conditions and media factors on R265 titan cell formation. A) The effect of cell density on cell enlargement was determined by growing

R265 cells in titan inducing conditions at varying concentrations (between 10^6 and 10^3 cells/mL, as indicated) and cell size being measured 24hrs later (percentages indicate proportion of the population >15 µm). Maximum cell enlargement capacity (B), budding index (C) and ploidy (D) of R265 cells in RPMI at 10^6 cells/mL (high density growth) at 37°C with 5% CO_2 for 24 hr and 7 days. Budding index was expressed as percentage of budded cells per total number of cells. At least >3000 cells were analysed for each sample from two independent repeats and significance was determined by one-way ANOVA (****=p<0.0001). Cells recovered from 7 day high density induction cultures were analysed for ploidy (orange) which was consistent with a 1C and 2C haploid DNA content as found for the YPD grown cells (red). E) Microscopy images depicting the budding index of cells grown in YPD (left panel), RPMI for 24hr (middle panel) and RPMI for 7days (right panel). Scale bar: 10µm. F) Impact of temperature and 5% CO_2 growth: cell body diameter of R265 cells after 24hrs of growth in RPMI with 5% CO_2 at 37°C or 30°C. The effect of RPMI-specific compounds on R265 titan cell formation (G,H). RPMI-specific amino acids (L-Glutamic acid, L-Aspartic acid, L-Arginine, L-Glutathione, L-Asparagine and L-Proline) were added to DMEM either at the concentration used in RPMI ('low conc.') or two-fold higher ('high conc.') and tested for their capacity to trigger titan cell formation after 24 hr induction at 37ºC in 5% CO_2 G). RPMI-specific compounds (Vitamin B12, Biotin, and para aminobenzoic acid (pABA) were supplemented to DMEM at the levels present in RPMI and then evaluated for their capacity to induce titan cell formation after 3 days incubation at 37ºC in 5% CO_2 H). The graphs are representation of 3 biological repeats and statistical significance was determined by one-way ANOVA, where ****=p<0.0001.

Impact of temperature and CO_2 on Titan cell formation

Cryptococcus responds to human physiological temperature (37°C) by exhibiting a variety of morphological changes including capsule elaboration, cell body enlargement and cell shape

alteration [13, 30, 31]. Hence, we investigated the role of temperature on R265 yeast-titan cell transformation by comparing cells grown in the presence of 5% CO_2 at either 37°C or 30°C. At 30°C incubation, no titan cells were generated and the median cell body size [5.03µm (1.04-12.85)] was significantly lower than at 37°C [11.17µm (4.04-28.6)] (Fig 6B). Thus, elevated temperature is essential to produce titan cells in our *in vitro* protocol.

The most dramatic biological response of *Cryptococcus* to CO_2 is capsule biosynthesis which occurs concurrently with cell body enlargement [16, 28, 29]. Consequently, we compared cells grown at 37°C in 5% CO_2 with those grown under normal atmospheric conditions at 37°C. Relative to growth in 5% CO_2, the proliferation of R265 was significantly inhibited in ambient atmosphere [Mean CFU: CO_2=28.5 x10^5 cells/mL vs CO_2- free 0.29 x10^5 cells/mL; ($p<0.001$)] and no titan cells were observed in this condition (Fig. S2). Thus, both elevated temperature and high CO_2 are required for *in vitro* titan cell formation.

P-aminobenzoic acid is a major trigger of titanisation in RPMI

While comparing the titan induction capacity of RPMI against DMEM media, we noticed that the giant cell phenotype emerged in RPMI but not DMEM. This raised the hypothesis that either RPMI is enriched with a trigger of titan cell formation that is lacking in DMEM, or that DMEM contains a factor that suppresses titan cell formation. Since RPMI and DMEM media have a close chemical composition, we took advantage of this similarity and sequentially supplemented DMEM with RPMI-specific compounds with the aim of identifying an RPMI-specific factor that triggers titanisation in R265 cells. Compared to RPMI, DMEM lacks the capacity to produce giant cells after 24 hr (Fig. 6G) and generates a much lower proportion (13.7%) when the induction period is prolonged to 3 days (Fig. 6H). RPMI differs from DMEM in its amino acid composition and so we first supplemented DMEM with 'RPMI-specific'

amino acids (L-Glutamic acid, L-Aspartic acid, L-Arginine, L-Glutathione, L-Asparagine and L-Proline) either singly (data not shown) or as a mixture. However, none of these conditions were sufficient to confer titan-inducting capacity to DMEM, even when supplemented at twice their normal concentration (Fig. 6G). Based on these results, we conclude that amino acid availability is not the trigger for R265 titanisation.

We continued by testing three additional compounds that are present in RPMI but absent from DMEM: Vitamin B12, Biotin, and para-aminobenzoic acid (pABA). Whilst vitamin B12 or biotin supplementation into DMEM had relatively little effect, addition of pABA significantly increased the production of titan cells from 13.7% to 29.0% (median cell diameter =11.94µm vs 12.82 µm, $p < 0.0001$) (Fig. 6H). Consequently, pABA appears to be a major trigger for titan cell formation in RPMI.

Finally, we noted that supplementary iron (in the form of Iron (III) nitrate nonahydrate-Fe $(NO_3)_3.9H_2O$) is present in DMEM but absent from RPMI. We therefore tested whether iron availability may actively inhibit titanisation. Indeed, adding iron to RPMI (Fe $(NO_3)_3.9H_2O$+RPMI) slightly reduced the induction capacity of RPMI by ~4%. In summary, therefore, the efficient induction of titan cells in RPMI likely results from the combined presence of pABA and the absence of supplementary iron.

Strain specificity

There is considerable evolutionary divergence between clades within the *Cryptococcus* genus and indeed the nomenclature of this group is rapidly changing in recognition of potential cryptic species [32]. To begin to assess variation in titanisation capacity, we screened 25 different cryptococcal isolates comprising 15 *C. gattii* species complex strains (VGI – VGIV), 8 *C. neoformans* strains (VNI and VNII) and 2 *C. deneoformans* strains (VNIV) for their

capacity to form titan cells in our *in vitro* protocol (3 days incubation in RPMI with 5% CO_2 at 37°C). Overall, the capacity to form titan cells in *C. gattii* strains was significantly higher than either *C. neoformans* or *C. deneoformans.* All 15 *C. gattii* strains produced titan cells, with an average of 73% titan cells at the end of the assay (Table 1). In contrast, only 4/8 (*C. neoformans*) and 0/2 (*C. deneoformans*) strains showed any level of titanisation (Table 1). Within the *C. gattii* species complex, VGII genotype strains (*C. deuterogattii*) displayed the highest titanisation capacity (averaging 79.0%) while VGI (*C. gattii*) scored the lowest at 64.8% (Table 1).

Table 1**. Capacity profile for titan cell formation among cryptococcal isolates.** Percentage of titan cells was determined based on capacity to enlarge >10µm (Fig. S3) and having >2C ploidy (Fig. S4)

Species/strain	**Genotype**	**Median size [size range] (µm)**	**% Titan cells***
C. gattii			
WM265	VGI	10.9 [4.1-28.4]	62.7
WM179	VGI	11.3 [4.1-25.0]	67
	Av. of VGI	**11.1**	**64.8**
R265	VGIIa	13.4 [5.1-29.6]	79.7
CDDR271	VGIIa	12.9 [4.4-26.5]	84.7
ENV152	VGIIa	10.6 [5.5-28.0]	54.8
ICB180	VGII	12.7 [3.4-26.3]	82.6
CBS10089	VGII	13.3 [5.6-25.1]	89.1
CDCR272	VGIIb	13.5 [6.8-39.2]	90
B7735	VGIIb	12.9 [5.5-26.3]	86.4
EJB18	VGIIc	11.3 [4.7-19.5]	75.6
EJB52	VGIIc	11.1 [4.8-19.5]	68.3
	Av. of VGII	**12.3**	**79**
CBS6955	VGIII	8.24 [4.34-17.9]	66.3
CBS6993	VGIII	9.9 [4.8-22.6]	45.7
	Av. of VGIII	**9.1**	**56**
WM779	VGIV	11.8 [4.2-25.5]	66.5
CBS1010	VGIV	12.6 [4.3-22.2]	80
	Av. of VGIV	**12.2**	**73.2**
All *C. gattii* (Average)		**10.75**	**73.3**

C. neoformans			
H99	VNI	7.7 [3.4-20.1]	21.3
ZC1	VNI	7.6 [4.46-15.9]	5.8
ZC8	VNI	12.4 [5.4-20.7]	76.1
ZC12	VNI	4.1 [2.1-7.0]	0
CBS8336	VNI	9.6 [4.6-24.8]	39.9
125.91	VNI	7.2 [4.6-16.3]	7.9
	Av. of VNI	**8.1**	**23.8**
TU_406_1	VNII	10.0 [4.9-18.5]	0
HAMDANC 3-1	VNII	9.3 [4.5-22.1]	0
	Av. of VNII	**9.6**	**0**
All *C. neoformans* (Average)		**9.7**	**18.8**
(AVERAGE)			
B3501	VNIV	7.2 [4.5-17.43]	0
CBS6995	VNIV	4.5 [3.4-11.1]	0
	Av. of VNIV	**5.85**	**0**
All *C. deneoformans* (Average)		**5.85**	**14.2**

382

383 **Titanisation in *C. gattii* is a polygenic trait**

384 Several genetic regulators have been implicated in the control of titanisation in *C. neoformans*
385 [6, 7, 13, 15, 33]. The interaction between these (nuclear genome-encoded) genetic regulators
386 and mitochondrial activity has been proposed [22]. Consequently, we exploited a collection of
387 parent/progeny crosses that we generated as part of an earlier study, and for which
388 mitochondrial genotype is known, [34] to begin to investigate the genetic control of titanisation
389 in *C. gattii*. Mitochondrial genotype and inheritance was confirmed by the expression of *ATP6*
390 gene (encoded by the mitochondrial genome) [34].

391 Firstly, we investigated a cross between *C. gattii* R265 and *C. gattii* LA584, a strain that
392 belongs to the same VGII group as R265 but shows a significantly lower capacity to titanise in
393 our *in vitro* conditions (Fig 7A). The progeny from this cross showed considerable variation in
394 titanisation capacity, although none exceeded the titanisation capacity of R265. Ploidy
395 measurement of parents/progeny based on flow cytometry analysis of DAPI staining for DNA

396 content is shown in Fig. S5. Notably, there was no correlation between titanisation capacity of
397 individual progeny and the mitochondrial genotype (R265 or LA584) that they had inherited,
398 suggesting that mitochondrial genotype is not a major driver of this phenotype.

399

400 We then turned our attention to a cross between R265 and a more distantly related strain, B4564
401 (VGIII), which shows relatively low levels of titanisation. In this outgroup cross, a 100%
402 inheritance of the mitochondrial genome from B4564 (*MAT***a**) was confirmed in 18 progeny
403 [34]. Despite this uniparental mitochondrial inheritance, all the progeny exhibit a significantly
404 higher capacity for titanization than B4564 (Fig. 7B). Ploidy measurement of parents/progeny
405 based on flow cytometry analysis of DAPI staining for DNA content is shown in Fig. S5.
406 Furthermore, 12/18 progeny showed a higher capacity for titanisation than either parent
407 ($p<0.0001$) with 5 progeny (P1, P5, P7, P8, P9 and P18) showing a remarkable >95% titan cell
408 population by the end of the assay. Together, these data suggest that the nuclear genome, and
409 not the mitochondrial genome, is the major source of variation in the capacity of different
410 isolates to form titan cells.

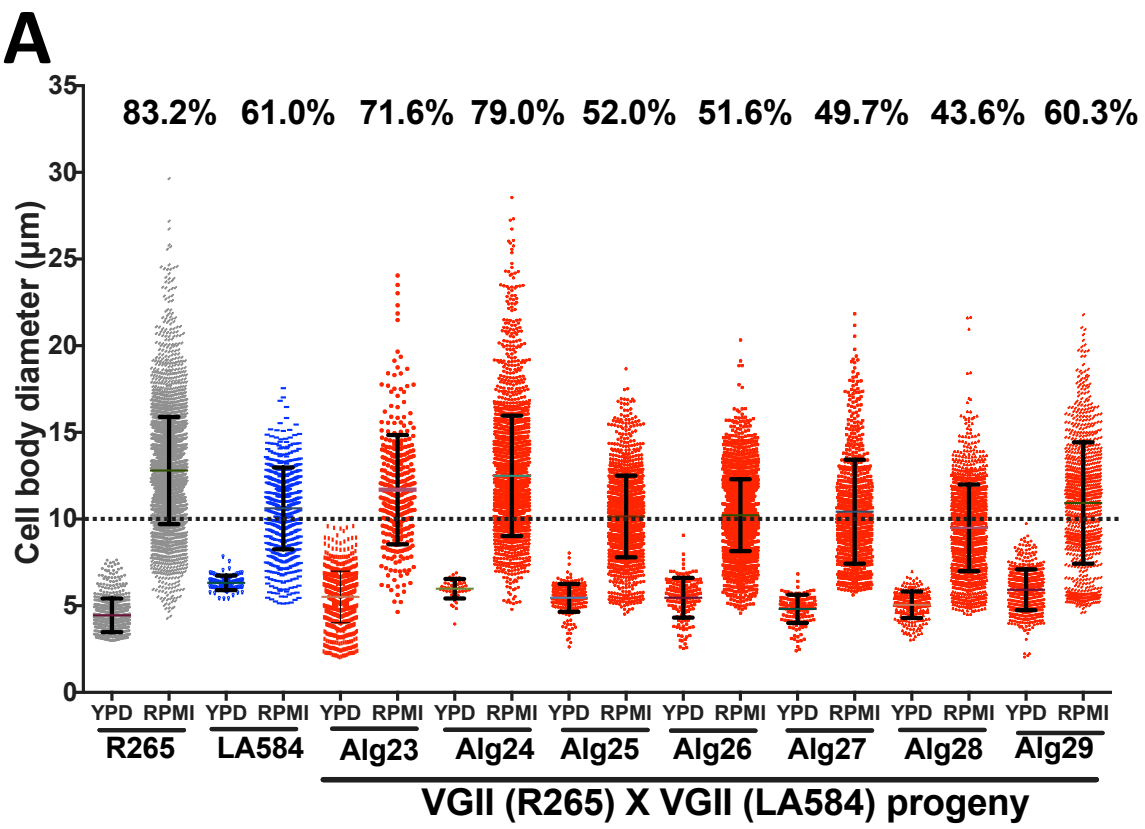

411

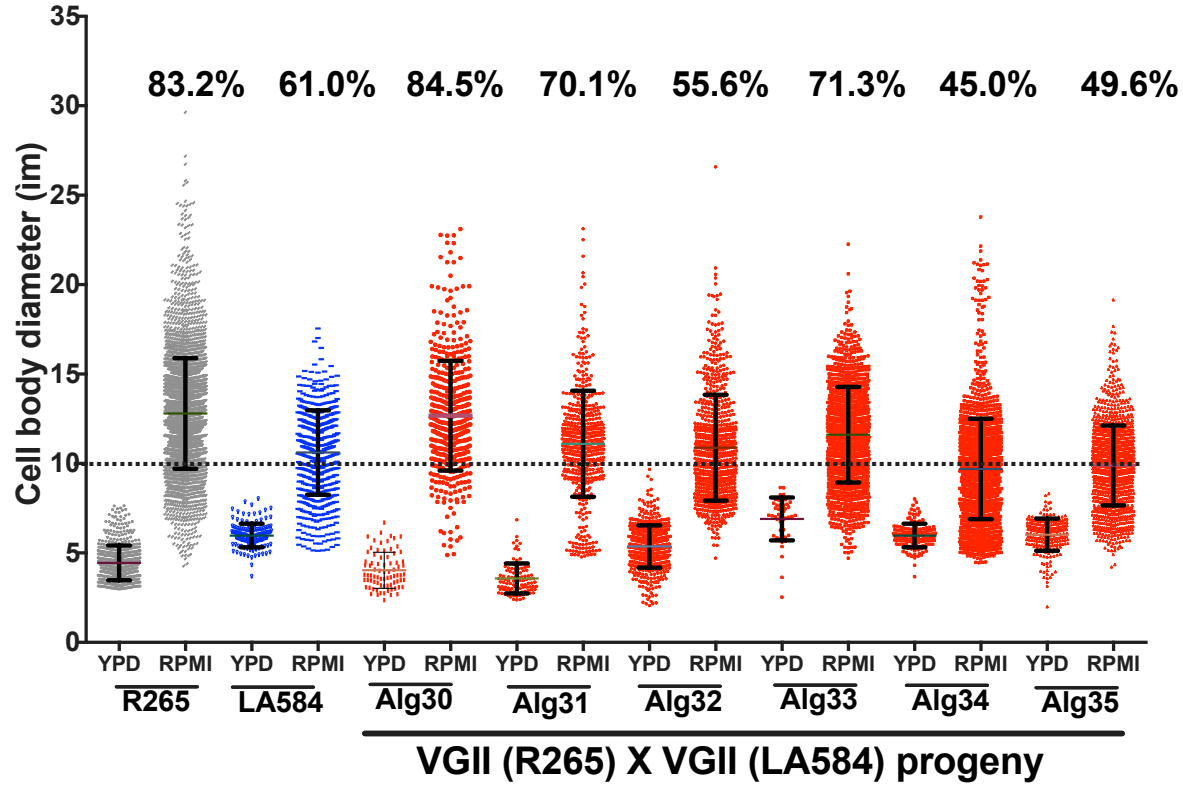

412

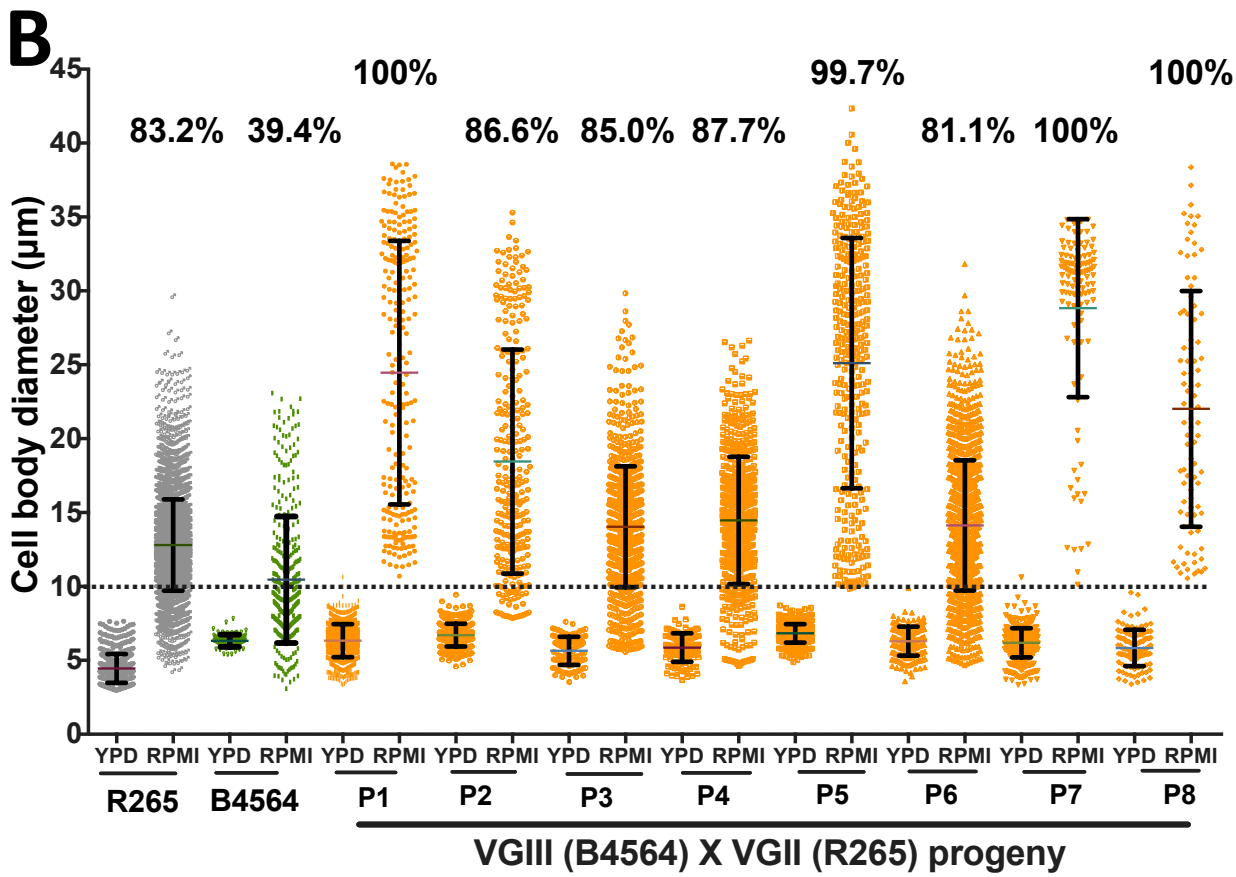

413

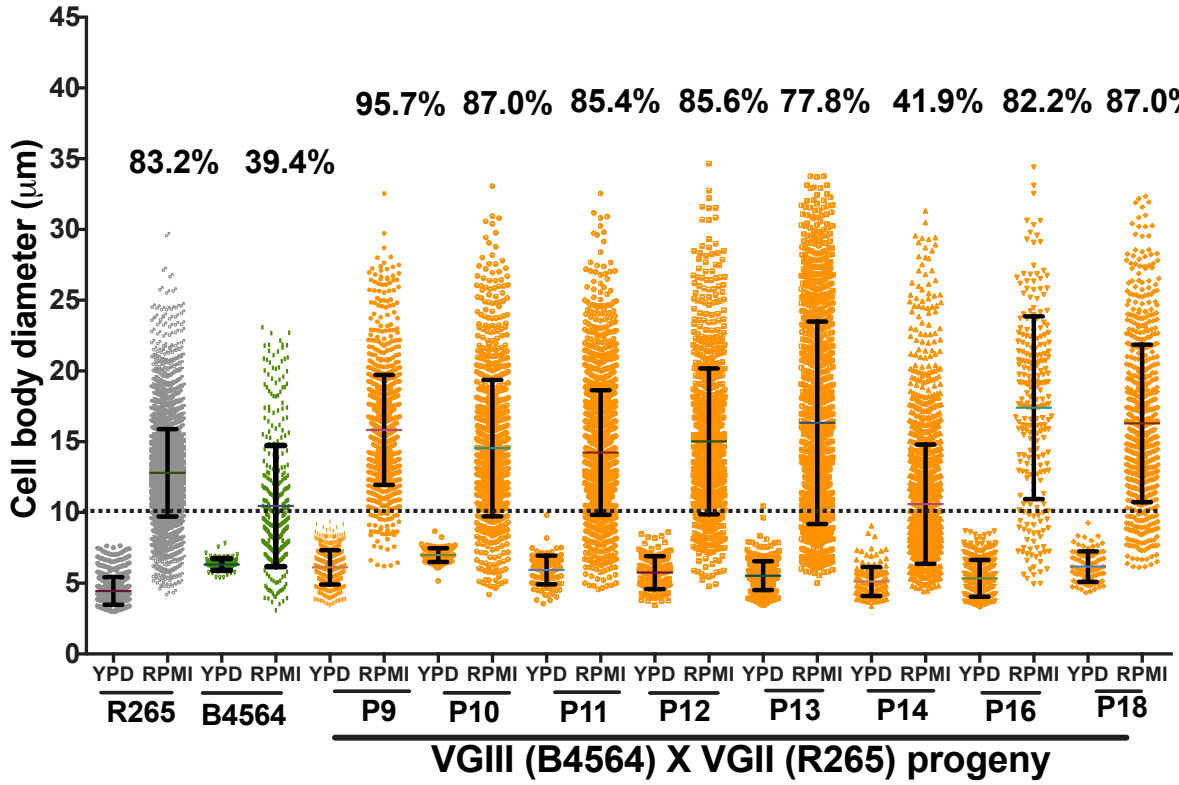

414

Figure 7 Titan cell formation capacity of *C. gattii* progeny arising from two crosses. (A) Titanisation pattern following three days of induction for R265 (VGII) x LA584 (VGII) and 13 progeny (Alg23-Alg35) arising from this cross [34]. (B) Titanisation pattern following three days of induction of R265 (VGII) x B4564 (VGIII) and 18 of the progeny (P1-P18) arising from this cross.

Discussion

Cryptococcus adaptation to the host environment is accompanied by phenotypic, metabolic and genetic alterations that are essential for pathogenicity [13, 35-41]. Typically measuring 5-7 µm, the cryptococcal yeast cell can undergo a morphological switch in the lungs to form enlarged polyploid titan cells, which have been studied *in vivo* [6, 7] and recently induced *in vitro* [13-15].

Here we report a new *in vitro* model for induction of *bone fide* titan cells. Our protocol is a one-step incubation of cryptococcal cells in serum-free RPMI media with 5% CO_2 at 37ºC and is therefore highly amenable to high-throughput screens.

Using our *in vitro* protocol, we conducted a detailed analysis of titanisation in the *C. gattii* strain R265 (VGIIa). We show that R265 titan cells induced *in vitro* possess enlarged cell body size, a large central vacuole, thick capsule and cell wall, and were polyploid after 5 days. Consequently, they exhibit all the hallmarks of true titans produced during mammalian infection. Unlike other cryptococcal strains, however, R265 shows a separation between size and ploidy increase. We suggest that the asynchronous progression of these two events may be due to R265 undergoing

cell size increase without passage through the cell cycle and then subsequently switching to DNA replication once the critical volume has been attained.

The lack of synchronisation between cell enlargement and DNA replication is a major difference between R265 titan cells and other well-studied *Cryptococcus* titan cells [6, 7, 13, 14, 20, 22, 26]. We suggest that the asynchronous progression of these two events is due to the prolonged time the titan cells spend in the G1 phase and/or cell cycle arrest at the G1/S checkpoint. This is supported by the ploidy of the 24 hr induction samples, where the vast majority of cells show a 1C DNA content. In yeast, a late G1 cell cycle arrest, known as "Start", is part of the core cellular response to stress [42, 43].–In R265 we observe that cell enlargement occurs before polyploidization during the early period of induction, so that the enlarged cells remain as 1C haploid yeast cells for the first two days of induction. By day 3 of induction, the enlarged cells begin to duplicate their DNA content to at least 2C but almost completely stop budding at the same time [budding index: 2.8% (26/933)] (Fig 3C). This leads to a major distinction between the species, in that *C. neoformans* titan cells can produce daughter cells within our *in vitro* titan induction model (Fig. S6) whilst C. *gattii* R265 titans do not. We note that this observation may be of value in studying cell cycle dynamics in *Cryptococcus* species (particularly *C. gattii*), since producing synchronised cryptococcal populations for such investigations has previously been methodologically challenging.

To explain the unbudded phase of the induced cells, we attempt to correlate this phenotype with cell cycle progression with reference to *C. neoformans*. In *C. neoformans*, large unbudded G2 cells have been shown to emerge during a stationary growth phase [44]. Recently, while scrutinizing the cell cycle regulation of titan cells in *C. neoformans*, Altamirano *et al* [25] described a two-step process of titanisation: a) typically-sized cells duplicate DNA to 2C and arrest in G2 as unbudded cells; and b) then the cells are released (by the combined influence of

the cell cycle gene Cyclin Cln1 and "stress signals") to form polyploid titan cells. Contrary to this phenomenon, R265 cells exhibit an actively budding phase in the early period of induction where the majority of the cells display 1C DNA content consistent with G1 and then undergo DNA replication to form G2 arrested unbudded polyploid titan cells at the later time point (day 5 onwards) where the 1C DNA content is totally lost (Fig. 5B). In agreement with this observation, we observed that the transcriptional profile of cells undergoing titanisation mirrors their cell-cycle phenotype. Consequently, the budding and mitosis genes, *CDC11* and *CLN1,* were expressed early and peaked at 24hrs (a point at which budding is prevalent and most cells have a 1C DNA content), suggesting that the cells were predominantly in either G1 or M phase. *CLN1* is required for releasing *C. neoformans* titan cells from G2 arrest (during cell cycle progression) [25] and therefore it is not surprising for that *CLN1* is downregulated at day 3 (Fig. 5B) when the budding index drops significantly. However, it is intriguing that *CLN1* is partially upregulated at day 5 and 7. In *C. neoformans, CLN1* forms a critical balance between DNA replication and cell division [25]. Our data suggest that *CLN1* is involved in the regulation of cell division during the first 24 hr of induction and in DNA replication during the unbudded phases at 5 and 7 days. Although we did not study cell cycle regulation of *C. neoformans* titan cells, *C. neoformans* titans generated via our *in vitro* system differ from R265 titan cell by profusely budding after 3 days of induction (Fig. S6). *C. neoformans* titan cells can pass through the G2/M checkpoint (G2/M transition), commit to mitosis and produce buds [6, 7, 13, 15].

We also demonstrate that R265 titan cells produce daughter cells with a polyploid DNA content similar to their mother cells. In contrast, *C. neoformans* titan cells produce both haploid and aneuploid progeny [20], with sizes ranging between 5-7µm and 2-4µm respectively [13, 45]. Given that population heterogeneity in *C. neoformans* is associated with preferential dissemination to the CNS [46, 47], it is possible that this lack of heterogeneity in *C. gattii* may

491 contribute to the differences in disease etiology in this species. In particular, murine models
492 have shown that *C. neoformans* isolates that produce high percentage of titan cells fail to
493 disseminate to the brain and instead remain in the lung, consistent with pneumonia or chronic
494 infection [48, 49]
495
496 The fact that RPMI, but not the very similar cell culture medium DMEM, induced R265 titan
497 cells enabled us to identify p-Aminobenzoic acid (pABA) as a major driver of titanisation. The
498 mechanism by which pABA does this remain unclear at present. However, we note that pABA
499 is an antifungal metabolite that has efficacy against several fungal plant pathogens such
500 *Fusarium graminearum*, *Magnaporthe oryzae*, *Rhizoctonia solani, Sclerotinia sclerotiorum*
501 and *Valsa ambiens var. pyri*. [50]. Since titanisation is linked to the fungal stress response, it
502 may be that low dose p-ABA induces a mild stress that triggers titanisation. In this context
503 modulation of the cell cycle and morphogenesis of *Colletotrichum fructicola* (a plant fungal
504 pathogen) by pABA has been documented [51]. Alternatively, pABA's well documented role
505 in oxidative damage tolerance [52] and the role of reactive oxygen species in titan cell induction
506 [23] may suggest a role for reactive oxygen balance in this phenomenon.
507
508 Finally, using our *in vitro* protocol, we evaluated the capacity for titan cell formation between
509 and within cryptococcal species. We found titanisation was particularly abundant within *C.*
510 *gattii* /VGII (*C. deuterogattii*). Interestingly, Fernandes and colleagues reported a similar cell
511 enlargement phenotype while screening for clinically relevant attributes in *C. gattii* [17]. To
512 start to dissect the genetic regulation of this process, we tested and analysed the titanisation
513 profile of a collection of parent/progeny crosses that we generated in our previous study [34].
514 It was striking to note the variation in this phenotype within recombinant progeny and, in
515 particular, the very high rates of titanisation found in the offspring of 'outgroup' hybrids. Most
516 of the progeny from this cross showed titanisation rates equal to or greater than that of R265

(the high titan cells generating parent). It is possible that this reflects a 'hybrid vigour' effect, resulting from the outcross. In the future, more detailed genomic investigation of these and other crosses may potentially facilitate a more comprehensive understanding of titan cell formation in this genus.

Overall, our titan induction protocol is an efficient and high throughput approach for producing titan cells at scale. By employing our *in vitro* protocol, we have discovered novel aspects of titanisation in *C. gattii* and revealed the separation of DNA replication and cell size increase. Together, we hope that this approach will provide a platform for the future mechanistic investigation of titanisation in this important group of pathogens.

METHODS

Cryptococcal strains and culture conditions

Cryptococcal strains used in this study are listed in Table 2. Prior to use, cryptococcal strains were maintained on Yeast Peptone Dextrose (YPD) (1% yeast extract, 2% bacto-peptone, 2% glucose, 2% bactor-agar) agar at 4°C from which overnight cultures were prepared in YPD broth at 25°C, 200rpm.

Table 2. Cryptococcal species and strains used in this study

Species and strains	Serotype	Genotype	Source
C. gattii WM265	B	VGI	Clinical isolate, Brazil
C. gattii WM179	B	VGI	Clinical isolate, Australia
C. gattii R265	B	VGIIa	Clinical isolate, Vancouver, Canada

C. gattii CDCR271	B	VGIIa	Clinical isolate, immunocompetent patient, Kelowna, British Columbia, Canada
C. gattii ENV152	B	VGIIa	Environmental isolate, Alder tree, Vancouver Island, Canada
C. gattii ICB180	B	VGII	Environmental isolate, Eucalyptus tree, Brazil
C. gattii CBS10089	B	VGII	Clinical isolate, Brazil
C. gattii CDC272	B	VGII	Clinical isolate, Greece
C. gattii B7735	B	VGIIb	Clinical isolate, Vancouver, Canada
C. gattii EJB1	B	VGIIb	
C. gattii EJB52	B	VGIIc	Clinical isolate, Oregon, USA
C. gattii CBS6955	B	VGIII	Clinical isolate, Oregon, USA
C. gattii CBS693	C	VGIII	Clinical isolate, USA

C. gattii LA584	B	VGII	Clinical isolate, Colombia
C. gattii B5464	C	VGIII	Clinical isolate, USA
C. gattii WM779	C	VGIV	Clinical isolate, USA
C. gattii CBS1010	C	VGIV	Veterinary, South Africa
C. neoformans H99	B	VGIV	Clinical isolate, USA
C. neoformans Zc1	A	VNI	
C. neoformans Zc8	A	VNI	Clinical, Zambia
C. neoformans Z12	A	VNI	Clinical, Zambia
C. neoformans 125.91	A	VNI	Clinical, Tanzania
C. neoformans Tu369-2	A	VNI	Environmental isolate, Mopane tree bark, Botswana
C. neoformans HAMDANC 3-1	A	VNII	Pigeon droppings, Belo Horizonte, Brazil
C. neoformans B3501	D	VNIV	Clinical isolate, usa

C. neoformans CBS6995	D	VNIV	Clinical isolate, USA
C. neoformans CBS8336	A	VNI	Wood of Cassia tree, Brazil

536

537 ***In vitro* induction of Titan cells**

538 Yeast cells from overnight cultures were collected (by centrifugation at 4000 r.p.m for 2 mins),
539 washed three times with phosphate buffered saline (PBS), re-suspended in 3mL PBS and
540 counted on a haemocytometer to determine cell densities [53, 54]. Except where otherwise
541 noted, titan induction was achieved by inoculating $5x10^3$ yeast cells in 1 mL serum free-RPMI
542 1640 within a 24 well tissue culture plate for 24 hours to 21 days at 37°C in 5% CO_2 without
543 shaking.

544

545 For generation of daughter cells, the 7 day old titan-inducing culture was passed through a
546 >20µm cell strainer and >20µm-sized Titan cells were re-cultured in YPD overnight. Then, the
547 daughter cells were isolated by filtering the overnight culture using a 15µm cell strainer and
548 collecting the flow-through.

549

550 **Cell size measurement**

551 Cells recovered from titan induced or YPD grown cultures were washed in PBS and fixed with
552 50% methanol. After Indian ink staining for capsule visualization, cellular images were
553 obtained using a Nikon TiE microscope equipped with phase-contrast 20X optics. Cell body
554 and capsule sizes for individual cells were measured by using ImageJ software in combination
555 with automated measurement based on Circle Hough Transformation algorithm [55].

556 **Cell wall and capsule**

Cells were fixed with 4% methanol-free paraformaldehyde for 10 mins and stained with calcofluor white (CFW, 10 µg/ml) for another 10 mins [13]. Total chitin was determined by flow cytometry on an Attune NXT instrument, with quantification of CFW staining using FlowJo software. For capsule visualization, cells were counterstained with India Ink (Remel; RMLR21518) and images acquired using a Nikon TE2000 microscope and analysed using ImageJ software.

DNA content measurement Ploidy

RPMI and YPD grown cells were recovered, washed 3x in PBS, fixed in 50% methanol and stained with 3 ug/ml DAPI at 10^5 cells/mL. For each sample, about 10000 cells were acquired on an Attune NXT flow cytometer and the result was analysed using FlowJo v. 10.7.1. Cells were sorted for doublet and clump exclusion by using FSC-A vs FSC-H gating strategy and compared to control, YPD grown, yeast cells.

RNA extraction and purification

Total RNA extraction was performed on uninduced (YPD grown) and titan-induced R265 cells by employing the protocol of QIAGEN (RNeasy Micro Kit [50]); Cat. No./ID74004) with slight modification. Samples of overnight YPD grown R265 cultures and titan-induced cells of the different time-points (24 hr, 72 hr, 5 days and 7 days) were harvested, washed three times in PBS, adjusted to ~10^6 cells/mL and pelleted in 1.5mL Eppendorf tubes. The cell pellets were flash-frozen in liquid nitrogen and stored at -80°C overnight. The cells were lysed by mixing in 400µL of RNAase, transferring to a 2 mL lysing tubes (MP Biomedicals™ 116960100) and beating with a bead beater (MP Biomedicals 116004500 FastPrep 24 Instrument Homogenizer) for thorough cell disruption. The homogenized sample was centrifuged for 3 min at 10,000 xg at room temperature. The aqueous portion was separated, mixed with 70% ethanol at 1:1 ratio

and transferred to an RNeasy Mini Spin Column. Finally, RNA extraction and purification were carried out as described in manufacturer's protocol.

RT-qPCR and gene expression analysis

The extracted RNAs from YPD grown and titan-induced samples were reversed transcribed (RT) to cDNA by using FastSCRIPT™ cDNA Synthesis protocol (Catalogue Number: 31-5300-0025R]. In brief, 15µL of RNA samples were mixed with 1µL of RTase and 4µL of FastSCRIPT™ cDNA Synthesis Mix (5X) before 30 min incubation at 42ºC and subsequent 10 min incubation at 85ºC. Quantitative PCR for the selected putative cell cycle genes was determined for each RT samples by mixing 2µL of the RT samples with 38µL master mixed of KAPA enzyme (KABA SYBR FAST qPCR Kits) and designed primers (table S1) and run in a real-time PCR detection system (CFX96 Touch Real-Time PCR Detection System; Ref. no. :1845096). Gene expression level was obtained and normalized according to change difference with the housekeeping gene, *GAPDH*. Finally, the relative expression profile was expressed as a function of comparative threshold cycle (C_T) by using the follow formula (III):

I. Delta $C_T = C_{T\,gene} - C_{T\,GAPDH}$

II. Delta delta $C_T = C_{Tgene}$-average Delta C_T

III. Relative gene expression= $2^{-\text{delta deltaCt}}$

References

1. May, R.C., et al., *Cryptococcus: from environmental saprophyte to global pathogen.* Nat Rev Microbiol, 2016. **14**(2): p. 106-17.
2. Bielska, E. and R.C. May, *What makes Cryptococcus gattii a pathogen?* FEMS Yeast Res, 2016. **16**(1): p. fov106.
3. Kwon-Chung, K.J., et al., *Cryptococcus neoformans and Cryptococcus gattii, the etiologic agents of cryptococcosis.* Cold Spring Harb Perspect Med, 2014. **4**(7): p. a019760.
4. Cooney, N.M. and B.S. Klein, *Fungal adaptation to the mammalian host: it is a new world, after all.* Curr Opin Microbiol, 2008. **11**(6): p. 511-6.
5. Ballou, E.R. and S.A. Johnston, *The cause and effect of Cryptococcus interactions with the host.* Curr Opin Microbiol, 2017. **40**: p. 88-94.
6. Okagaki, L.H., et al., *Cryptococcal cell morphology affects host cell interactions and pathogenicity.* PLoS Pathog, 2010. **6**(6): p. e1000953.

7. Zaragoza, O., et al., *Fungal cell gigantism during mammalian infection.* PLoS Pathog, 2010. **6**(6): p. e1000945.
8. Feldmesser, M., Y. Kress, and A. Casadevall, *Dynamic changes in the morphology of Cryptococcus neoformans during murine pulmonary infection.* Microbiology, 2001. **147**(Pt 8): p. 2355-65.
9. Okagaki, L.H. and K. Nielsen, *Titan Cells Confer Protection from Phagocytosis in Cryptococcus neoformans Infections.* Eukaryotic Cell, 2012. **11**(6): p. 820.
10. Crabtree, J.N., et al., *Titan cell production enhances the virulence of Cryptococcus neoformans.* Infect Immun, 2012. **80**(11): p. 3776-85.
11. Cruickshank, J.G., R. Cavill, and M. Jelbert, *Cryptococcus neoformans of unusual morphology.* Applied microbiology, 1973. **25**(2): p. 309-312.
12. Love, G.L., G.D. Boyd, and D.L. Greer, *Large Cryptococcus neoformans isolated from brain abscess.* Journal of clinical microbiology, 1985. **22**(6): p. 1068-1070.
13. Dambuza, I.M., et al., *The Cryptococcus neoformans Titan cell is an inducible and regulated morphotype underlying pathogenesis.* PLoS Pathog, 2018. **14**(5): p. e1006978.
14. Trevijano-Contador, N., et al., *Cryptococcus neoformans can form titan-like cells in vitro in response to multiple signals.* PLoS Pathog, 2018. **14**(5): p. e1007007.
15. Hommel, B., et al., *Titan cells formation in Cryptococcus neoformans is finely tuned by environmental conditions and modulated by positive and negative genetic regulators.* PLoS Pathog, 2018. **14**(5): p. e1006982.
16. García-Rodas, R., et al., *Cryptococcus neoformans capsular enlargement and cellular gigantism during Galleria mellonella infection.* PLoS One, 2011. **6**(9): p. e24485.
17. Fernandes, K.E., et al., *Species in the Cryptococcus gattii Complex Differ in Capsule and Cell Size following Growth under Capsule-Inducing Conditions.* mSphere, 2016. **1**(6): p. e00350-16.
18. Fernandes, K.E., et al., *Phenotypic Variability Correlates with Clinical Outcome in Cryptococcus Isolates Obtained from Botswanan HIV/AIDS Patients.* mBio, 2018. **9**(5): p. e02016-18.
19. Okagaki, L.H., et al., *Cryptococcal titan cell formation is regulated by G-protein signaling in response to multiple stimuli.* Eukaryotic cell, 2011. **10**(10): p. 1306-1316.
20. Gerstein, A.C., et al., *Polyploid titan cells produce haploid and aneuploid progeny to promote stress adaptation.* mBio, 2015. **6**(5): p. e01340-15.
21. *<The_Cryptococcus_neoformans_Titan_Cell_From_In_Viv.pdf>.*
22. Zhou, X. and E.R. Ballou, *The Cryptococcus neoformans Titan Cell: From In Vivo Phenomenon to In Vitro Model.* Current Clinical Microbiology Reports, 2018. **5**(4): p. 252-260.
23. Zhou, X., et al., *Host-derived Reactive Nitrogen Species mediate the Cryptococcus neoformans yeast-to-titan switch via fungal-derived superoxide.* bioRxiv, 2021: p. 2021.03.01.433276.
24. Mukaremera, L., et al., *Titan cell production in Cryptococcus neoformans reshapes the cell wall and capsule composition during infection.* The Cell Surface, 2018. **1**: p. 15-24.
25. Altamirano, S., et al., *The cyclin Cln1 controls polyploid titan cell formation following a stress-induced G2 arrest in <em>Cryptococcus</em&gt.* bioRxiv, 2021: p. 2021.08.24.457603.
26. Zaragoza, O. and K. Nielsen, *Titan cells in Cryptococcus neoformans: cells with a giant impact.* Curr Opin Microbiol, 2013. **16**(4): p. 409-13.
27. Zaragoza, O. and A. Casadevall, *Experimental modulation of capsule size in Cryptococcus neoformans.* Biol Proced Online, 2004. **6**: p. 10-15.
28. Mogensen, E.G., et al., *Cryptococcus neoformans senses CO2 through the carbonic anhydrase Can2 and the adenylyl cyclase Cac1.* Eukaryotic cell, 2006. **5**(1): p. 103-111.
29. Bahn, Y.S., et al., *Carbonic anhydrase and CO2 sensing during Cryptococcus neoformans growth, differentiation, and virulence.* Curr Biol, 2005. **15**(22): p. 2013-20.
30. Fries, B.C., et al., *Phenotypic switching in Cryptococcus neoformans results in changes in cellular morphology and glucuronoxylomannan structure.* Infect Immun, 1999. **67**(11): p. 6076-83.

31. Fuchs, B.B., R.J. Tang, and E. Mylonakis, *The temperature-sensitive role of Cryptococcus neoformans ROM2 in cell morphogenesis.* PloS one, 2007. **2**(4): p. e368-e368.
32. Hagen, F., et al., *Recognition of seven species in the Cryptococcus gattii/Cryptococcus neoformans species complex.* Fungal Genetics and Biology, 2015. **78**: p. 16-48.
33. Okagaki, L.H., et al., *Cryptococcal Titan Cell Formation Is Regulated by G-Protein Signaling in Response to Multiple Stimuli ∇.* Eukaryotic Cell, 2011. **10**(10): p. 1306-1316.
34. Voelz, K., et al., *Transmission of Hypervirulence traits via sexual reproduction within and between lineages of the human fungal pathogen cryptococcus gattii.* PLoS Genet, 2013. **9**(9): p. e1003771.
35. Kronstad, J., et al., *Adaptation of Cryptococcus neoformans to mammalian hosts: integrated regulation of metabolism and virulence.* Eukaryotic cell, 2012. **11**(2): p. 109-118.
36. Feldmesser, M., Y. Kress, and A. Casadevall, *Dynamic changes in the morphology of Cryptococcus neoformans during murine pulmonary infection.* Microbiology (Reading), 2001. **147**(Pt 8): p. 2355-2365.
37. Fries, B.C., et al., *Phenotypic switching of Cryptococcus neoformans occurs in vivo and influences the outcome of infection.* The Journal of clinical investigation, 2001. **108**(11): p. 1639-1648.
38. Li, Z. and K. Nielsen, *Morphology Changes in Human Fungal Pathogens upon Interaction with the Host.* Journal of fungi (Basel, Switzerland), 2017. **3**(4): p. 66.
39. Chang, A.L. and T.L. Doering, *Maintenance of Mitochondrial Morphology in Cryptococcus neoformans Is Critical for Stress Resistance and Virulence.* mBio, 2018. **9**(6): p. e01375-18.
40. May, R.C., et al., *Cryptococcus: from environmental saprophyte to global pathogen.* Nature reviews. Microbiology, 2016. **14**(2): p. 106-117.
41. O'Meara, T.R. and J.A. Alspaugh, *The Cryptococcus neoformans capsule: a sword and a shield.* Clin Microbiol Rev, 2012. **25**(3): p. 387-408.
42. Hartwell, L.H. and M.W. Unger, *Unequal division in Saccharomyces cerevisiae and its implications for the control of cell division.* The Journal of cell biology, 1977. **75**(2 Pt 1): p. 422-435.
43. Hartwell, L.H., et al., *Genetic control of the cell division cycle in yeast.* Science, 1974. **183**(4120): p. 46-51.
44. Takeo, K., et al., *Unbudded G2 as well as G1 arrest in the stationary phase of the basidiomycetous yeast Cryptococcus neoformans.* FEMS Microbiol Lett, 1995. **129**(2-3): p. 231-5.
45. Zhou, X., et al., *Host environmental conditions induce small fungal cell size and alter population heterogeneity in Cryptococcus neoformans</em&gt.* bioRxiv, 2020: p. 2020.01.03.894709.
46. Ngamskulrungroj, P., et al., *The primary target organ of Cryptococcus gattii is different from that of Cryptococcus neoformans in a murine model.* mBio, 2012. **3**(3): p. e00103-12.
47. Fernandes, K.E., et al., *Phenotypic Variability Correlates with Clinical Outcome in Cryptococcus Isolates Obtained from Botswanan HIV/AIDS Patients.* MBio, 2018. **9**(5).
48. Reuwsaat, J.C.V., et al., *The Transcription Factor Pdr802 Regulates Titan Cell Formation and Pathogenicity of Cryptococcus neoformans.* mBio, 2021. **12**(2): p. e03457-20.
49. Dambuza, I.M., et al., *The Cryptococcus neoformans Titan cell is an inducible and regulated morphotype underlying pathogenesis.* PLoS pathogens, 2018. **14**(5): p. e1006978-e1006978.
50. Laborda, P., et al., *Production of Antifungal p-Aminobenzoic Acid in Lysobacter antibioticus OH13.* J Agric Food Chem, 2018. **66**(3): p. 630-636.
51. Laborda, P., et al., *Antifungal Metabolite p-Aminobenzoic Acid (pABA): Mechanism of Action and Efficacy for the Biocontrol of Pear Bitter Rot Disease.* J Agric Food Chem, 2019. **67**(8): p. 2157-2165.
52. Lu, Z., et al., *Para-aminobenzoic acid (PABA) synthase enhances thermotolerance of mushroom Agaricus bisporus.* PloS one, 2014. **9**(3): p. e91298-e91298.

716 53. Smith, L.M., E.F. Dixon, and R.C. May, *The fungal pathogen Cryptococcus neoformans manipulates macrophage phagosome maturation.* Cell Microbiol, 2015. **17**(5): p. 702-13.
718 54. Olszewski, M.A., et al., *In Vitro Analysis of Metabolites Secreted during Infection of Lung Epithelial Cells by Cryptococcus neoformans.* Plos One, 2016. **11**(4).
720 55. Dragotakes, Q. and A. Casadevall, *Automated Measurement of Cryptococcal Species Polysaccharide Capsule and Cell Body.* J Vis Exp, 2018(131).
722